NINTH EUROPEAN ROTORCRAFT FORUM

PAPER NO. 6

A NEW APPROACH USING VORTEX POINT METHOD FOR PREDICTION
OF ROTOR PERFORMANCE IN HOVER AND FORWARD FLIGHT

B. Cantaloube and S. Huberson

September 13 - 15, 1983
STRESA - ITALY

A NEW APPROACH USING VORTEX POINT METHOD FOR PREDICTION

OF ROTOR PERFORMANCE IN HOVER AND FORWARD FLIGHT

by B. Cantaloube and S. Huberson

Abstract

We present a numerical unsteady method used for computing 3-D incompressible flows around helicopter-rotors. It is an extension of Rehbach's particles method to flow around surfaces with arbitrary motions. These surfaces are modelized by a surface doublet distribution and the vortex sheet by a set of vortex carrying particles. Some examples of applications to rotors are presented with a look at both kinematic and dynamic aspects of the flow.

1. Introduction

Numerical prediction of rotor performance seems to be one of the hardest attainable challenge for the aerodynamic engineer. Isolating the rotor from other solid boundaries constituting the helicopter or the ground, still leads to a configuration involving a lot of very complex problems. Each one of this problem appears to be at the frontier of actual numerical possibilities. If we have a look for example at the flow around a rotor in forward flight at a speed of about 40 m/s, different regions containing different difficulties can be reviewed.

From an aerodynamic point of view, the flow behaviour can be described as indicated on figure 1.

In a central region near the rotor axis, the flow is fully three-dimensional with frequently very important dissipative effects. Moreover, the wake of the blades interact strongly with the rotor axis, the real shape of which is far from simple.

In a second region, the flow can be more easily modelized and, due to the large aspect ratio of the blade, linear theory works quite well. Good results may also be expected from theories such as unsteady lifting lines, as developed by James, Van Holten, or Guiraud-Slama... Nevertheless, these theories have to be extended in order to account for the wake and blade interaction. An additional difficulty arise from the boundary conditions, especially between the different region.

Near the blade tip, we can find a third region (III) where the flow, on the advancing blade, can be transonic. In this subdomain, the fluid compressibility is determinent and we have to modelize its effect when computing the unsteady

flow in this region. A first approximation may be obtained from two dimensional calculations as those by Lerat-Sidès for example, or small perturbation transonic three-dimensional methods as developed by Chattot-Philippe. The account for the wake of the different blades remains very important.

Containing the blade tip, a last zone (IV) is found, where vortex phenomena must dominate, with the formation of a rolling up vortex sheet. There can be found supersonic conditions, with vortex/shock interaction.

Moreover, for such a rotor in forward flight, the cyclic pitch variation has to be added. This introduces one more difficulty due to variation of the grid path.

In this paragraphe, we do not account for the compressibility effect in transonic region. Recents studies particularly by Murman-Stremel show that it is possible to include within the classical incompressible vortex method a coupling with a transonic potential calculation. Most part of the existing methods are devoted to rotors in hover. Some of them have been developed within the background of propeller theories as the actuator disc of Rankine and Froude. In this early model, no account has been taken for the blade number, shapes are incidence. The first advanced theories are those developed by Betz, Goldstein. In these works, the authors study a class of propeller whose wake is an helicoïd with constant path. The load of each blade is obtained through analytical calculations.

The development of modern computers enables engineers to considerably improve these first methods. The more significant improvement was to account for the spanwise loading of the blade as an unknown of the problem. The wakes still remain described with a simplified geometrical shape in order to limit the number of freedom degrees. The Neuman problem on solid boundaries is then reduced to a linear system which is numerically solved. A lot of codes using those basic ideas are available and some recent versions are very sophisticated - Miller, Costes...

The last generation of computer codes can be illustrated by the work of Suma. In this method, the wake is entirely discretized in quadrangular panels and its position is computed so as to satisfy the classical kinematic condition, the circulation value of such element constituting the wake is evaluated through Kelvin theorem. The blade loading is obtained as a Neuman problem on the surface of the blades, or a Dirichlet formulation if thickness effect are retained. The resulting set of algebraic equations is solved by means of an iterative procedure. Some empirical parameters

are still introduced in the model, particularly for determining a correct position for the vortex line issuing from the blade tips. Moreover, the extension of the method to forward flight cases is not clear. A larger number of approximative treatments will probably have to be introduced if some attempt is made for such cases.

2. Theoretical background

In this chapter, the theoretical basis of Rehbach's vortex point method is recalled. Extension of this method to obstacles in arbitrary motion is then presented. In a last paragraph, we present an application to inviscid incompresible flow around an helicopter rotor.

2.1. Generalities and kinematic aspects

The problem we deal with can be split in two parts :
- the first one will concern solid boundaries modelization. These one are discretized with quadrangular elements and a piecewise constant doublet distribution.
- the second part will concern the non zero vorticity region ( ). The free vorticity distribution is discretized by vortex carrying particles.

These particles are shedded from the boundaries along given lines and their strengths and locations are determined through an emission model.

The induced velocity $\vec{V}_M$ at a given point M is calculated by using a Green identity. In this calculation, the whole vorticity distribution is taken into account : the free vorticity, and the attached vorticity via its equivalent doublet distribution

$$\vec{V}_M = \frac{1}{4\pi}\left\{ \iiint_\tau \vec{\pi}_P \wedge \nabla_P\left(\frac{1}{\overline{X_M - X_P}}\right) d\vec{\tau}_P - \iint_S \mu_P \nabla_M\left(\frac{(\overline{X_M \cdot X_P}) \cdot \overline{N_P}}{|\overline{X_M} - \overline{X_P}|^3}\right) dS_P \right\} + \vec{V}_\infty \quad (1)$$

All the vectors in this equation are given in a Galilean reference frame, and :

$\vec{V}_\infty$ is the upstream velocity
$\vec{X}_P$ is the integration point
$\vec{N}_P$ is the normal vector to the surface (S) at $\vec{X}_P$.

The doublet intensity μ is calculated by solving a Fredholm equation and taking into account the slip condition on solid boundaries :

$$\oint_S \mu_P \vec{N}_P \cdot \nabla_M \left(\frac{(\vec{X}_M - \vec{X}_P) \cdot \vec{N}_P}{|\vec{X}_M - \vec{X}_P|^3} \right) ds = -\iint \left[\vec{N}_L \frac{\vec{\Omega}_{P \wedge} \nabla_P \left(\frac{1}{\vec{X}_M - \vec{X}_P} \right)}{} \right] d\vec{\tau}_P - 4\pi \vec{V}_\infty \vec{N}_P \qquad (2)$$

where the surface integral is a Cauchy mean value integral. The time evolution of the free vorticity distribution is governed by Helmholtz equation :

$$\frac{D \vec{\Omega}_M}{Dt} = (\vec{\Omega}_M \cdot \nabla) \vec{V}_M \qquad (3)$$

where $\frac{D}{Dt}$ denotes the convective derivative with respect to time t. We obtain this equation by taking the curl of Euler equation. It represents a dynamic balance for any fluid particle.

It must be noted that the use of Helmholtz equation instead of Euler equation reduce our problem to a purely kinematic one.

Kelvin's theorem, governing the evolution of vortex filaments is automatically verified thanks to equation (3). Therefore, vorticity can be produced only from the boundaries which presently are supplied from experimental data.

In the particular case of an helicopter rotor blade, this reduces the vortex production model to the classical lifting surfaces model.

Let us consider the wake near the emission line. This line, in our case, reduces to the trailing edge. We can modelize this part of the vortex sheet by means of a doublet distribution μ. The well-known Kutta Jukovski condition -no pressure jump accross this surface- can be written

$$\frac{D \mu'}{Dt} = 0 . \qquad (4)$$

This equation is integrated on the surface, using the initial value of μ given by equation (2). The numerical discretization of (4) is achieved by transforming the doublet surface distribution in vortex carrying particles accordig to Rehbach's model.

At this stage, we can point out the importance of the emission pattern. This problem will be developed further for rotary wings in hovering flight.

For inviscid incompressible flows, the vortex carrying particles can be divided in two classes. The ones which never

have contact with solid boundaries and the others.

- The first class of particles only has a passive
role. They receive information from body surface and from the
second class of particles through relation (2)

- The second class of particles brings information
when leaving the body surface. This information is contained
in the vorticity carried by these particles and gives some
memory to the fluid.

A fixed wing in forward flight is moving away from the
emitted wake. Therefore, the wake disturbs for a relatively
short time the velocity field on the wing. A rotary wing wake
remains during a longer time close to the wing surface.
Moreover, the presence of the wake is the main cause for the
axial stream which characterizes such a flow. A straight
forward consequence will be necessity of very accurate
emission model.

The four fundamental sets for performing such a
calculation processed independently allow :

1) to work out, at each time step, the doublet
distribution μ by solving (2)
2) to create new vortex particles by means of (2) and
(4)
3) to remove the particles constituting the wake to
their new position (1)
4) to modify the carried vorticity for each particle
according to (3)

2.2. Dynamical aspect

The progression of such an unsteady calculation,
through the present method is generally split in two stages.

The first one, above described, deals only with the
kinematic aspect. It gives the velocity and vorticity field.
The transient period, from rest to a steady or periodic state
is in most practical cases of little interest. Therefore, it
can be shortened through different calculation techniques.

The second one involves the dynamical aspect of the
problem, particularly the pressure estimation within the flow
and the applied forces on the body surfaces. It does not
interfere anyway with the progression of the first stage.
Thus, it can be performed at the end of the transient period.

The pressure coefficient jump $[c_p]$, accross a lifting

surface S is given by :

$$\left[C_P\right] = \frac{2}{V_\infty^2}\left(\frac{\partial}{\partial t}\left[\varphi\right] + \vec{U}\cdot\nabla\left[\varphi\right]\right) \tag{5}$$

on S and $\left[\varphi\right]$ is the velocity potential jump. Moreover, $\left[\varphi\right]$ is given by the local doublet distribution μ . This yields :

$$\left[C_P\right] = \frac{2}{V_\infty^2}\left(\frac{\partial\mu}{\partial t} + \vec{U}\cdot\nabla\mu\right) \tag{6}$$

where $\vec{U}$ is defined by

$$\vec{U} = \frac{\vec{U}^+ + \vec{U}^-}{2}$$

and $\vec{U}^+$, $\vec{U}^-$ are the velocity on each side of (S). The explicit formulation of $\vec{U}$, thanks to (1), is given by :

$$\vec{U} = \frac{1}{4\pi}\left[\iiint_V\vec{\Omega}_{P\wedge}\nabla_P\left(\frac{1}{\overline{X_M-X_P}}\right)d\vec{v} + \iint_S\mu_P\nabla_P\left(\frac{(\vec{X_M}-\vec{X_P})\cdot\vec{N_P}}{(\vec{X_M}-\vec{X_P})^3}\right)ds\right] + \vec{V_\infty} \tag{7}$$

The time derivative of μ in the right hand member of (6) gives a convergence estimate when it goes to zero. It must be pointed out that this is not true for leading edge separation. In that case, this term does not vanish and modelize some viscous behaviour of the fluid.

We give here the general outline of a fully unsteady method. The main properties are :

- the realistic character of the convergence development, these calculations representing the transient period,

- the method is a step by step algorithm using only the four equations (1), (2), (3), (4) without any iterative process,

- the method does not need any experimental data input except the knowledge of the emission lines location.

Moreover, the discretization of the vorticity distribution by means of vortex carrying particles is of great advantage for the computation of very complicated flows. As an example, one can compare the flow pattern on figure 5-6-7 to the experiment done by Werlé, in the hydrodynamic tunnel

at ONERA. An other important point is that we are free of any eulerian grid, restricting the calculation to the domain where vorticity is not zero. This will considerably reduce the computational cost.

A last interesting feature is that, due to the use of Helmholtz's equation, we do not have to write any equilibrium condition on the vortex sheet surfaces. This is a great advantage since the pattern of vortex sheet is very complicated for most real flows. We only have to move a finite number of particles and to adjust the moduli and directions of the attached vorticities.

3. Application to helicopter rotors

Calculations are performed using the relative frame moving with one of the rotor blades. It is then easy to follow the rotor motion. The three axis of the calculation (x,y,z) are shown in fig. 2.

Let $\vec{V_r}$ be the velocity at point M in the relative frame. Then, we have the following relation

$$\vec{V_r} = \vec{V_a} - \vec{V_e} \tag{8}$$

where $\vec{V_a}$ is the absolute velocity in reference Galilean frame. It can be calculated using equation (2).

$\vec{V_e}$ is the driving velocity of the calculation frame :

$$\vec{V_e} = \vec{V_0} + \vec{\omega} \wedge (\vec{x_M} - \vec{x_0}) \tag{9}$$

where $\vec{\omega}$ is the blade instantaneous rotational velocity,
   $\vec{x_0}$ the rotor instantaneous center of rotation
and $\vec{V_0}$ the forward flight velocity.

In the blade attached frame the relative velocity of any particle is tangent to the body surface. Reporting equation (8) into equation (2) we can express this condition and we obtain a modified Fredholm's integral equation :

$$\iint_S \mu_P \vec{N_P} \cdot \nabla \left[\frac{(\vec{x_M} - \vec{x_P}) \cdot \vec{N_P}}{(\vec{x_M} - \vec{x_P})^3} \right] ds_P = -\iiint_V \vec{N_P} \cdot \left(\vec{\Omega_P} \wedge \nabla_P \left(\frac{1}{\vec{x_M} - \vec{x_P}} \right) \right) d\tau - 4\pi (\vec{V_\infty} - \vec{V_e}) \cdot \vec{N_P} \tag{10}$$

The doublet strength is a zero order tensor. So, it remains invariant in any arbitrary frame and the emission

condition is unchanged. The time evolution of the vorticity field $\vec{\Omega}$ is still obtained from Helmholtz's equation (3). This equation can be rewritten in the moving frame

$$\frac{d\vec{\Omega}_a}{dt} = (\vec{\Omega}_a \cdot \nabla)\vec{V}_a - (\vec{\omega} \wedge \vec{\Omega}_a) \cdot \qquad (11)$$

The same coordinate transform gives for the pressure coefficient jump :

$$[\Delta C_p] = \frac{2}{V_\infty^2}\left[\frac{\delta\mu}{\delta t} + \vec{U}_r \cdot \nabla\mu\right] \qquad (12)$$

where $\frac{\delta}{\delta t}$ is the time derivative for a fixed point in the moving frame. By adding the terms containing $\vec{V}_r$ to equation (7), we get an explicit expression for $\vec{V}_r$:

$$\vec{V}_r = \frac{1}{4\pi}\left[\iiint_V \vec{\Omega}_P \wedge \nabla_P\left(\frac{1}{\vec{X}_M - \vec{X}_P}\right)d\tau + \oiint_S \mu_P \nabla_P\left[\frac{(\vec{X}_M - \vec{X}_P)}{(\vec{X}_M - \vec{X}_P)^3}\right]ds + \vec{V}_\infty - \vec{V}_e \qquad (13)$$

It must be noticed that these modifications do not affect the four steps of the algorithm already described. The terms added to account for the moving frame are analytically integrated. So the evolution of each vortex carrying particle is obtained accurately.

3.1 Rotor Geometry

Most of applications presented here are relative to a three bladed-rotor. Such a rotor is currently used for wind-tunnell testing. So, its aerodynamic characteristics are well determined. The main geometrical parameters are given in fig. 2.

Each blade is represented by a zero-thickness surface twisted according to a linear law Θ (y/R), where Θ is the twist angle, y the spanwise coordinate and R the rotor-disc radius. We have the following expression :

$$\Theta(y/R) = \Theta_{0.7} - \Theta_v(y/R - 0.7) \qquad (14)$$

where $\Theta_{0.7}$ is the collective pitch angle, and Θ_v the linear

twist. Note that the twist axis is also for this case the y-axis of the moving frame.

The blade chord remains constant although the method allows more general geometrical shapes. The blade surface is divided into chordwise and spanwise rows of quadrangular surfaces. It results from this discretisation that the four equations to be solved readily reduce to sets of algebraic equations. From experimental knowledge of the flow, we can expect very large gradients at the blade tip. So, the grid will be stretched in this region in order to give a best account of the physical phenomena. The evolution of the chordwise discretisation will be given by a sinusoïdal law with respect to the y coordinate.

3.2 Pressure and resulting forces calculation

3.2.1 Pressure integration

The chordwise integration of the pressure jump gives the spanwise lift distribution $\mathcal{P}$. Thanks to the panelling of the blades this law will be a piecewise constant function of y. The resulting total circulation at each blade cross section is given by :

$$\Gamma(y) = \frac{\mathcal{P}}{\varsigma \, V_{\infty \varrho} \, L} \qquad (15)$$

where

$V_{\infty \varrho}$ is a local velocity $V_{\infty \varrho} = \| \vec{V}_o + \vec{\omega} \wedge \vec{y} \|$
$\vec{V}_o$ is the helicopter forward velocity,

3.2.2 Direct calculation :

For lifting surfaces, a body with a sharp trailing edge, the circulation Γ is directly related to the velocity potential jump along the trailing edge :

$$[\varphi_f] = \mu_f . \qquad (16)$$

The spanwise distribution of circulation can be given for potential flows by means of equation (15) :

$$\Gamma(y) = \mu_f . \qquad (17)$$

For a three-bladed rotors, we obtain the same results when

using equation (15) or (17), see fig. 10.

3.2.3. Dimensions and normalized coefficient

The circulation is usually adimensionalized using the blade tip velocity :

$$\bar{\Gamma}(y) = \frac{\Gamma(y)}{\omega R^2} \, . \tag{18}$$

From this equation we define the C_z coefficient :

$$C_z(y) = 2\bar{\Gamma}(y) \frac{(R/c)^2}{(y/c)} \, .$$

The thrust coefficient C_T which will be classically normalized using the rotor solidity σ :

$$\frac{C_T}{\sigma} = \text{thrust}/ {}_8 \pi R^2 (\omega R)^2 \sigma \, .$$

3.3 Adaptation to helicopter flow problems

3.3.1 Nested Meshes

For a practical use of the method, the most useful results are essentially those obtained in the last period of convergence, when a steady, or a periodic state is reached. Intermediate results which allow a refined analysis of the unsteady transition period are of less practical interest for design purpose. In that case, it can be of some interest to decrease the accuracy of the calculus during the early iteration steps. So, we have introduced in our algorithm a sequence of nested grids on the blade, these grids going more and more refined. The calculations are performed on each grid until a converged solution is obtained, then we construct an interpolate for the blade loading. All the geometrical parameters representing the blade are set to the new correct values, and new emission points are defined. The discretization of the wake, which has been already formed, remains unchanged. Thus, we obtain a wake model in which all the emission lines did not contain the same number of vortex point.

Numerical experimentation confirms that such a process did not introduced any instability in the calculations and that only a few time steps are necessary to recover the steady state with this new mesh. On figure 3 an example of the beginnning of a calculus is shown, exhibiting the change of blade meshes. The velocity field projected in a plane containing the axis of the rotor is given in figure 4.

Three different meshes have been used during this
sequence. The tip vortex formation is very well illustrated
in this case.

3.3.2 Periodicity conditions for hovering cases

This paragraph deals with the problem of a rotor
impulsively started in a fluid initially at rest. This kind
of calculation is an essential test case for validation and
further development of any new method since, as it has been
pointed out in the introduction, existing codes are mainly
concerned with this flow. Two main difficulties are described
here after. First, we try to extensively use the periodicity
of the flow in order to save computing time. The second
difficulty encountered was to accurately calculate the early
stage of the flow with the growing of the starting vortex
ring.

It is well-known that the computation of the
doublicity distribution at the surface of an obstacle leads to
solve a set of linear equations which can be written :

$$A_{ij}\mu_j = N_i \cdot U_i \qquad (21)$$

where μ_j is the local value of the doublicity distribution,
at X_j. N_i is the normal to the boundary at X_i , and U_i the
velocity induced in X_i by the whole vortex system. For a
multibladed rotor, we can introduce the matrix M^k
corresponding to the frame change from the frame relative to
the kth blade to a reference one which will be noted $k = 0$.
Then, it must pointed out that the velocity field U_i depends
on the doublet distribution which is constant from a blade to
another. Furthermore, U_i dependance on the vortex wake ω^k
of a blade is linear in the Biot-Savart law. So, it can be
written :

$$U(X_i) = A_s^k(X_i, X_j^k)(\mu_j^k) + B_s^k(X_i, X_j^k)(\Omega_j^k) \qquad (22)$$

where A_s and B_s are matrices. If the flow is periodic, one
can define some matrices B_s^k using M^k,

$$B_s^k = B_s(X_i, X_j^k) = B_s(X_i, M^{k-1}X_j) \qquad (23)$$

or

$$\Omega_j^k = M^{k-1}\Omega_j \ . \qquad (24)$$

Let us now have a look at the Biot-Savart integral law.

A single vortex point ω_j located in X_j will induce at point X_i a velocity given by the equation :

$$U(X_i) = \Omega_j \wedge \frac{(X_i - X_j)}{|X_i - X_j|^3} \tag{25}$$

Let us change in these formulae X_j for X_j^k, ω_j for ω_j^k, we obtain :

$$U(X_i) = \Omega_j^k \wedge \frac{(X_i - X_j^k)}{|X_i - X_j^k|^3} = M^{k-1}\Omega_j \wedge \frac{(X_i - M^{k-1}X_j)}{|X_i - M^{k-1}X_j|^3} \tag{26}$$

from (27), (28) we found that

$$(X_i - M^{k-1}X_j) = M^{k-1}(M^k X_i - X_j) \tag{27}$$

and

$$M^{k-1}\Omega_j \wedge \left[M^{k-1}(M^k X_i - X_j)\right] = M^{k-1}\left[\Omega_j \wedge (M^k X_i - X_j)\right] \tag{28}$$

so finally

$$U(X_i) = \frac{M^{k-1}\left[\Omega_j \wedge (M^k X_i - X_j)\right]}{|M^k X_i - X_j|^3} \quad . \tag{29}$$

All the process can be repeated when calculating the deformation term :

$$U(X_i) = \sum_k \left\{ M^{k-1}\left[A_s^0(M^k X_i, X_j)\mu_j + B_s^0(M^k X_i, X_j)\Omega_j\right] \right\} \tag{30}$$

and, if we separate the μ_j and ω_j contributions :

$$\sum_k \left\{ M^{k-1}\left[A_s^0(M^k X_i, X_j)\right] \right\}\mu_j = \sum_k M^{k-1}\left[B_s^0(M^k X_i, X_j)\Omega_j\right] \tag{31}$$

The first interest of this form, illustrated on figure 4, will be that only one blade and his wake are calculated, and the velocity field at a given point is calculated by applying to this point successive rotation, and to the obtained value of the velocity the inverse rotation. So very few changes have to be done to transform a single-bladed rotor code into a multibladed rotor one. The use of equation (17) projected on the normal N_i gives a linear system for calculating μ which is of the same order to the system encountered for the one-bladed rotor cases.

3.3.3 Transient period calculation

The flow around a rotor in hover is very similar to that encountered around propellers, at least when the stream is supposed to be axial. This condition is necessary to have a periodic flow. However, a fundamental difference is encountered at the starting of the rotation. In the rotor case, we start with no axial velocity. This fact lead to the creation of a very strong vortex ring which will remain near the rotor disc for a long time. A careful computation of this transient period is necessary to obtain an accurate solution. This is a restraining phenomenon which significatively affects the computing time for the smaller value of the axial velocity. On figure 5 we present a comparison between a starting vortex ring obtained in the hydrodynamic tunnel of ONERA by Werlé, and our calculations with the same three bladed rotor. A good qualitative agreement is obtained.

On figures 6 and 7, the calculated flow pattern observed during this early stage is shown. We indicate the vortex ring location, compared to the rotor-disc position. It can be pointed out that in a first stage, the vortex ring is going downstream, but is then sloved down by the following blade and thrown upstream. At this time, an axial stream begin to flow near the axis under the rotor-disc. However, many rotor turns will be necessary before the starting vortex ring to be swept downstream.

So, reinforcing the algorithm efficiency will necessitate the introducion of a few technique whose aim will be to help the natural flow to make the influence of this vortex ring rapidly decaying.

A first method consists in supressing the impulsive start, using instead an empirical solution similar to that which is used by Suma. The essential difference will be that we use this law, only to have a realistic first approximation of the wake. Then the flow is supposed to go on and new particles are created. The particles constituting the portion

of the wake empirically constructed are moved according to
Helmholtz equation. In this algorithm, it can be pointed out
that even this last part of the wake satisfies, partially,
the fluid dynamics equations. This is an easy way to
eliminate the starting vortex ring. Unfortunately, spurious
instabilities are introduced when matching the empirical wake
-given by Landgrebe law- and the newly created wake. This is
coming from the path of the helicoïd corresponding to
Landgrebe Law. This one is constant and the path
corresponding to the new wake is not constant and somewhat
different. So, we use a smoothing function in this part of
the wake. Applying this algorithm with a coarse mesh of only
eight elements on the blade, we obtain after ten time steps
the results given in figure 8 for the spanwise loading of the
blade. These results compare quite well to those calculated
by Suma.

The triangular element which can be observed at the
blade tip was degenerated to avoid a too large number of
emission points in this region. All the other elements being
very long, we can supposed that the calculation, except near
the tip, look like a lifting line calculation and so large
time steps can be chosen. But in the tip region, the mesh is
refined, and special process, such as this triangular
element, have to be introduced if one want to use these large
time steps.

Another way to eliminate the starting vortex ring can
be implemented. It consists in using an axial velocity which
will be progressively set to zero. The flow near the rotor
disc is then rapidly regularized. One of the most interesting
aspects of such a method is that we can observe strong
unsteady effect during the velocity decreasing period.

A last method to start the calculation has been
tested. It consists in reproducing a numerical analogous to
the starting of a real helicopter rotor.

We start the rotation with an incidence angle which
minimize the thrust. The angle of attack is then
progressively set to the desired value. This way is a very
reducing one since it is a good numerical representation of
the real physical phenomenon. On figure 9 we indicate the
convergence history for each one of these two last methods.

3.4 Numerical results

3.4.1 Rotor in Hover, Velocity field and spanwise
loading.

The results presented here have been obtained using the technique of decaying axial wind. On figure 10a we give the wake pattern projected in the x,y plane. Each represented point corresponds to a vortex carrying particle. The velocity value at each "vortex point" is also represented here. Figure 10b is the same wake projected in a plane normal to the rotor disc. This plane is periodically encountered by each blade. So, the vortex ring initiated at the blade tips is clearly illustrated there. These results are obtained after only three revolutions of the rotor. At this stage, there still remains a small axial wind which ratio to the blade tip velocity is $\beta = 0.07$.

One can identify very clearly on this figure some of the different regions described on figure 1. The blade shank vortex ring is carried array slowly compared with the blade tip vortex. It results in a recirculating zone near the blade shank. More details about its incidence on the spanwise loading will be given later. The slipstream contraction appears very clearly on this figure as well as regions II and III of figure 1.

The calculated spanwise loading is given in figure 11. A satisfying agreement with Suma results can be observed. However, the recirculating zone near the blade shank increases the local circulation.

On figure 12, we give the results obtained for a two-bladed rotors of which geometrical characteristics are :

$$\begin{array}{rl}
\text{blade aspect ratio :} & 13.7 \\
\text{Linear twist :} & -11^{\circ} \\
\text{Collective pitch :} & = -9.8^{\circ}
\end{array}$$

A good agreement is also observed for this case with numerical results obtained by Crespin. The recirculating phenomena observed in the preceding case did not appear so clearly here. This must be related to the blade shank which is very closed to the rotor axis.

3.4.2 Forward flight application

Since the wake is built in our method through a real physical process of evolution, no major modification is needed to calculate forward flight cases. Here, we restrict ourselves to the case of a rotor plunged in a uniform stream whose direction does not coincide with the rotor axis. This is not a common property with current other methods which need the "a priori" introduction of an empirical wake which is iteratively set to an equilibrium position.

The only problem encountered will be caused by the cyclic pitch variation which affect each blade independently. The result of this will be that the rotor is no more a single solid. So the matrix representing it is no longer constant. The linear system to be solved when calculating the blades loading introduced a different computation at each time step and this requires a very large computing time. The matrix cannot be preconditioned at the beginning of the calculations, for example in a triangular form. In order to preserve the algorithm efficiency, we introduce a non-centered scheme for the time integration. The loading of a blade depend on the others blade loading only at the previous time steps. So, for solid blades which correspond to the same matrix A_s^0, the problem reduce to the appropriate use of several transforms. Introducing the following notation for the time dependence of a given function f :

$$f(t_0 + n \Delta t) = f^{(n)}$$

we get :

$$\left[A_s^0 (x_i, x_j^{(n+1)}) \mu_j^{(n+1)} \right] \cdot N_i = \left\{ - \sum_{k \neq i} M^{i,k-1^{(n)}} \left[A_s^0 (M^{i,k} x_i^{(n)}, x_j^{(n)}) \right] \mu_j^{k^{(n)}} \right.$$

$$\left. + \sum_k M^{i, k-1^{(n)}} \left[B_s^k (M^{i,k} (x_i)^{(n)}, x_j^{(n)}) \Omega_j^{i^{(n)}} \right] \right\} \cdot N_i \qquad (32)$$

where $M^{i,k}$ is a matrix representing the transform of the blade k in the blade i. Each blade remains rotating but has no common axis with the others, the A_s^0 matrices are all the same and represent the same obstacle geometry thanks to an isometric tranform. This is not true for the Bio-Savart Law which must be applied to wakes with entirely differing shape. However, it appears that a good solution is to use for each wake the moving frame corresponding to its emitting blade.

Finally let us notice that the process can be extended to all elements of the mesh of a blade. This allows to treat cases such as moving boundaries, and flexible blades. Due to the proximity of the surface elements, some fixed point iterations could be necessary to obtain a good solution.

On figure 13 we present results obtained with a single-bladed rotor in forward flight. This is an exploratory results. We indicate the blade position on the rotor disc in the small circle above the C_z curve. An inflexion point, not existing for the first period, can be remarked. It must correspond to the passage of the blade above its own wake. The emission line deformation on the two sides of the wake compare very well with the two vortex cores observed by Werlé

in hydrodynamic visualization. Since the non-centered time integration scheme allows to reduce a multi-bladed rotor to several single-bladed rotors, we can expect very good results for the present method for such cases.

CONCLUSION

We have just presented here a numerical method applied to prediction of multi-bladed rotor performances in hover. Moreover, in its actual form, the code allows to compute a one-bladed rotor in forward flight case. Two main features are to be noted :

- the Lagrangian variables allow to have no grid in the wake
- the fundamental steps, described in paragraph 2 are performed independently.

This gives a great versatility to our method. Therefore, we can hope an easy extension to real flight configurations, including multi-bladed rotors in forward flight, flexible blades and cyclic pitch variations. The wake discretization by means of vortex carrying particles, unlike doublet panels, allows an easier account for the shearing effect observed when the wake encounters other solid boundaries such as the helicopter body, ground.... The periodicity condition and the results obtained with the decreasing axial wind will allow the adaptation of our code to many other rotary wing problems such as propellers, with any number of blades.

A next important step would be to include thickness effects. To this purpose, we plan to use the Dirichlet interior formulation presently developed at ONERA by Rehbach.

REFERENCES

1)   E.C. James: Lifting line theory for an unsteady wing as a singular perturbation problem.
     J. Fluid Mech, $\underline{70}$, p. 753, 1975.

2)   Van Holten: Some notes on unsteady lifting line theory.
     J. Fluid Mech. $\underline{77}$, p. 561, 1976.

3)   J.P. Guiraud, and G. Slama: Sur la théorie asymptotique de la ligne portante en régime incompressible oscillatoire.
     La Rech. Aerosp. 1981-1, p. 1.

4) A. Lerat, and J. Sidès: Numerical simulation of
    unsteady transonic flow using the Euler equations in
    integral form.
    Israel J. Techn.   , p. 302, 1979.

5) J.J. Chattot, and J.J. Philippe: Calcul des réparti-
    tions de pression sur une pale d'hélicoptère
    symétrique en vol d'avancement à portance nulle.
    La Rech. Aérosp. 1980-5, p. 317.

6) W.J. Rankine: On the mechanical principles of the
    action of propellers.
    Trans. Inst. of Naval Architects., Vol. 6, 1865

7) R.E. Fraude: On the part played in propulsion by
    differences of fluid pressure.
    Trans. Inst. of Naval Architects., Vol. 30, 1889.

8) A. Betz: Screw propellers with minimum loss of energy.
    Nachrichten der K. Gesellschaft der Wissenschaften zu
    Göttingen, 1919.

9) S. Goldstein: On the vortex theory of screw
    propellers.
    Royal Society Proceedings, 123, 1929.

10) R.H. Miller: Rotor blade harmonic air leading.
    AIAA Journal 2, n° 7 p. 1254, 1964.

11) J.J. Costes: Application du concept de ligne portante
    au calcul des pales d'hélicoptères.
    La Rech. Aerosp. 1978-6, p. 355.

12) R. Dat: Représentation d'une ligne portante animée
    d'un mouvement vibratoire par une ligne de doublets
    d'accélérations.
    La Rech. Aérosp. n° 133, 1969.

13) S.G. Sadler: A method for predicting helicopter wake
    geometry, wake induced flow and wake effects on
    airloads.
    American Helicopter Society 27th Annual National Forum
    Washington, D.C. May, 1971.

14) S.M. Beldserkowskii: Calculation of the flow about
    wings of arbitrary planform at a wide range of angles
    of attack.
    R.A.E. Library trans. 1433 (1970) - Mekhanika
    Zhidkosti I Gaza 4 p. 32, 1968.

15)   J.M. Suma: Advanced rotor analysis methods for the
        aerodynamics of vortex/blades interactions in hover.
        8th European Rotorcraft and Powered lift aircraft
        forum, 1982.

16)   C. Rehbach: Calcul Instationnaire de Nappes
        tourbillonnaires émises par des surfaces portantes
        fortement inclinées.
        (AGARD CP 247 n° 14), 1978.

17)   H. Werlé, and C. Armand: Mesures et visualisations
        instationnaires sur les rotors.
        6ème colloque A.F.I.T.A.E., 1969.

18)   A.J. Landgrebe: The wake of a hovering helicopter
        rotor and its influence on rotor performance.
        American Helicopter Society, 28th Annual National
        Forum Washington, D.C. May, 1972.

19)   C. Rehbach: Numerical calculation of three-dimensional
        unsteady flows with vortex sheet.
        AIAA, 16th Huntsville, January 10, 1978, 78-111.

20)   Y. Crespin: Unsteady Rotor aerodynamic using a vortex
        panel method.
        AIAA 9th Atmospheric flight mechanics conference,
        August 9-11, 1982, San Diego, 82-1348.
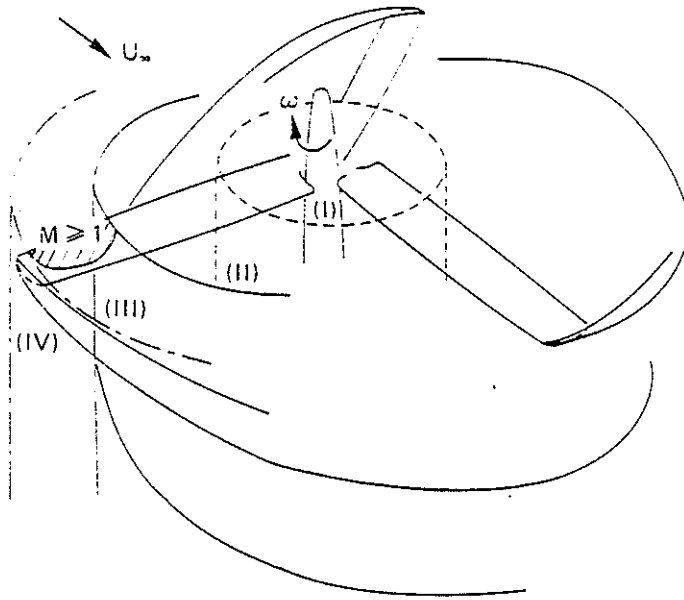
Fig. 1 — Schematic of hovering rotor wake structure.
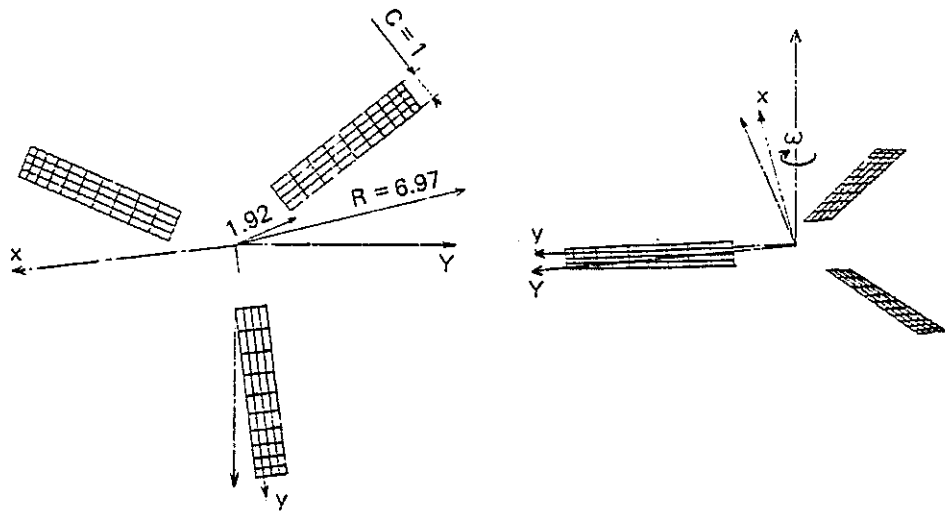
Fig. 2 — Rotor geometry.
a) Characteristic dimensions
b) Inertial and blade attached frames.
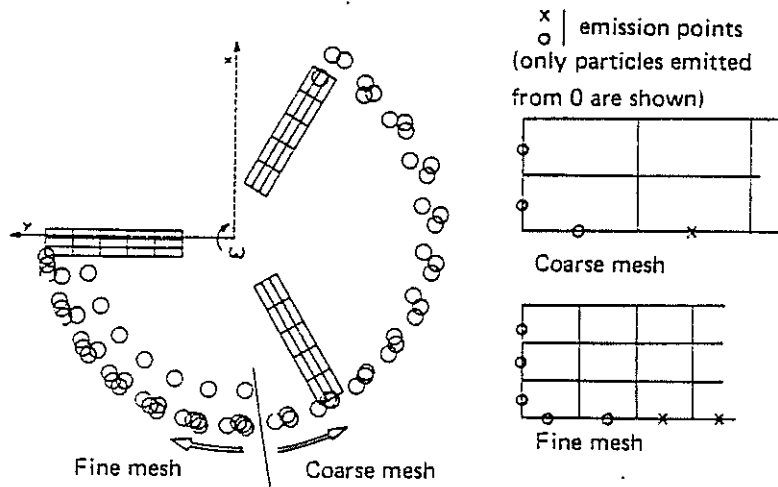
Fig. 3 — Division of the emission lines in a calculation with nested panellings.
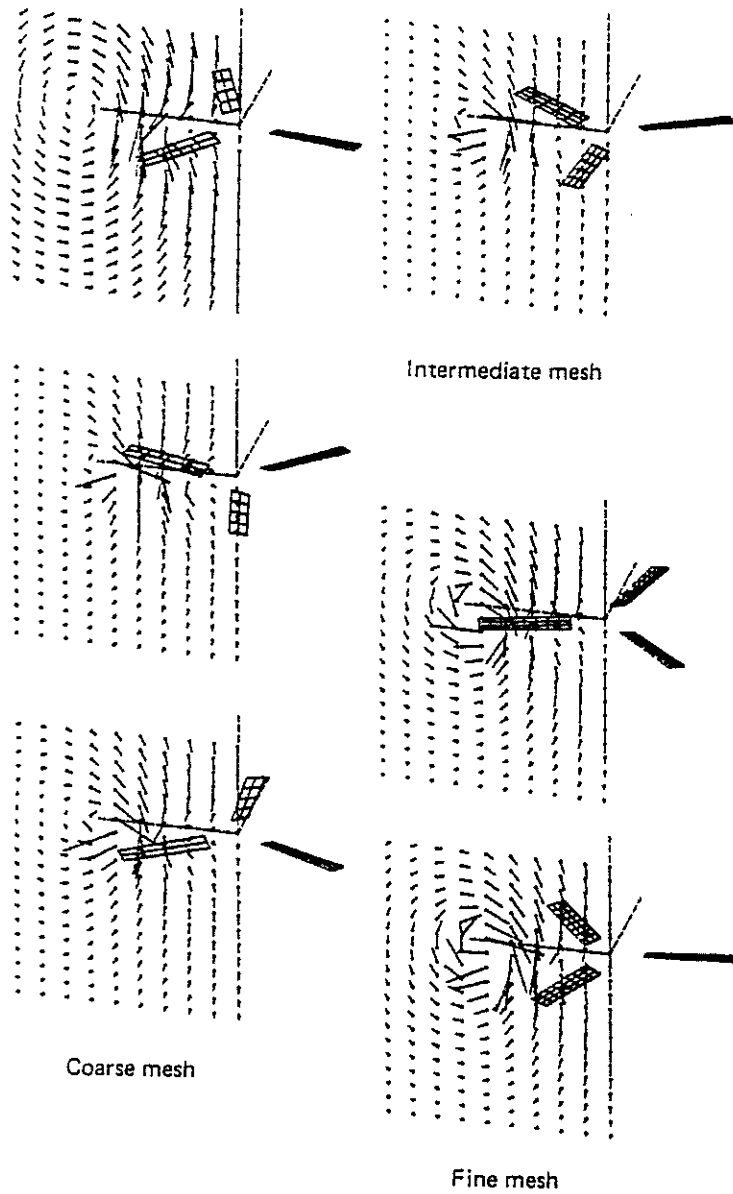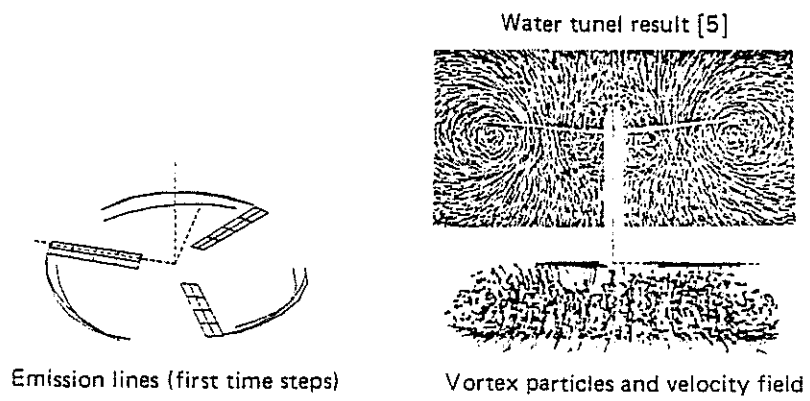
Intermediate mesh

Fig. 4 — Nested panelling technique.

Coarse mesh

Fine mesh

Water tunel result [5]

Emission lines (first time steps)

Vortex particles and velocity field

Fig. 5 — Three-bladed rotor in hovering flight.

Tip vortex

Cross section

Starting vortex

Rotor cross section

Present method
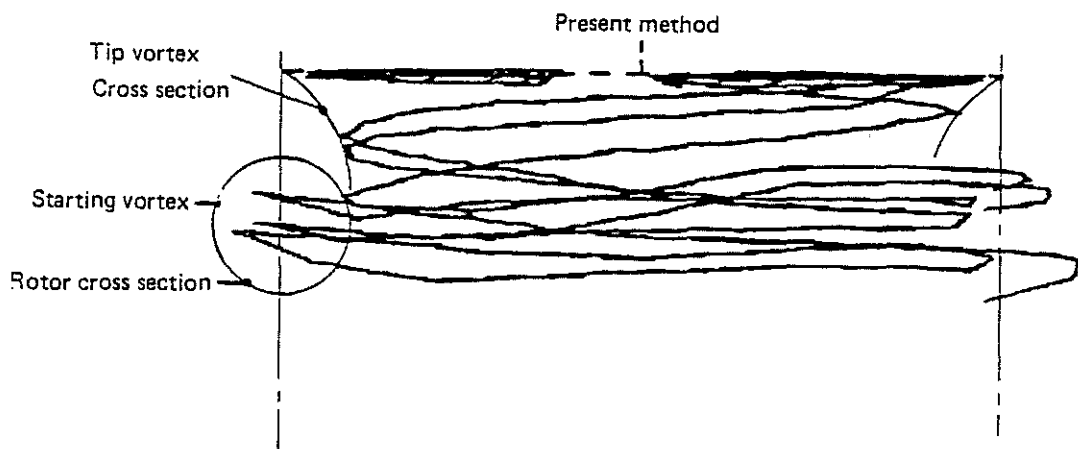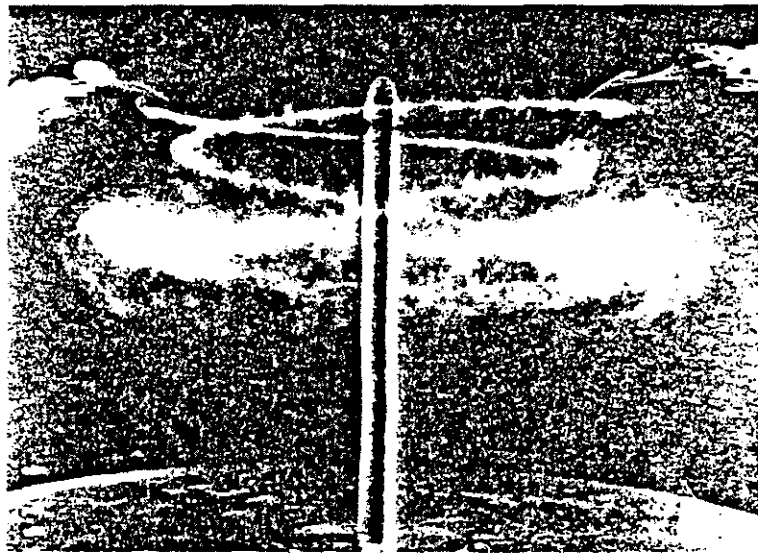
Fig. 6 — Rotor starting in hovering flight.
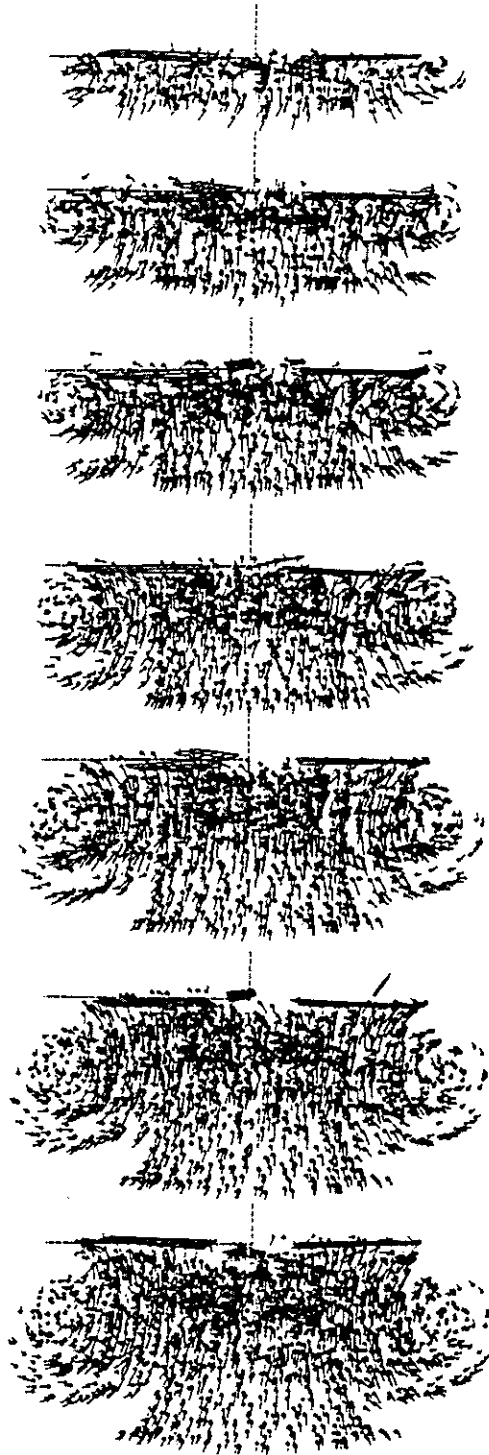
Fig. 7 — Starting vortex at different time-step.
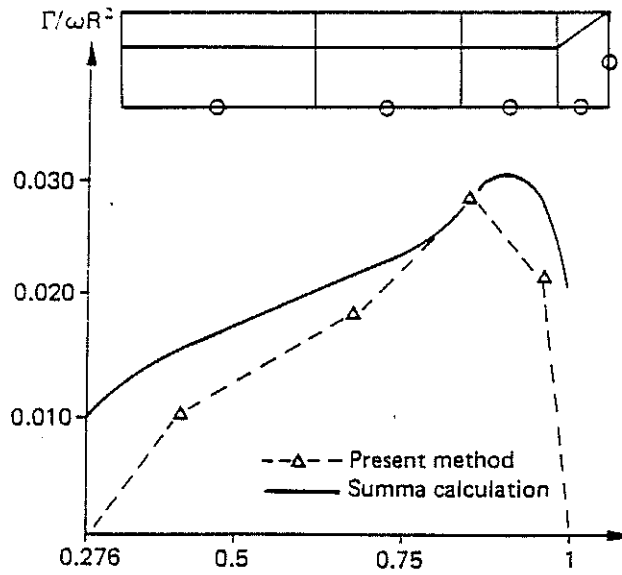
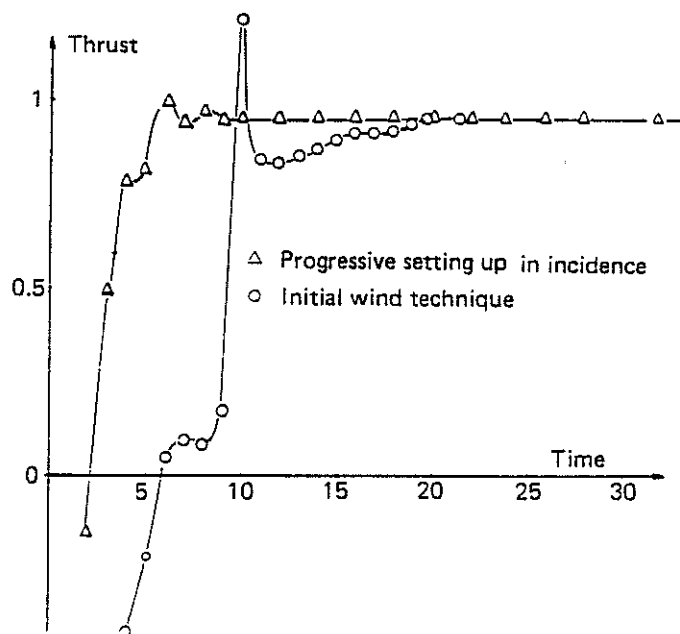*Fig. 8 — Sectional-loading for a one-bladed rotor in hovering flight.*
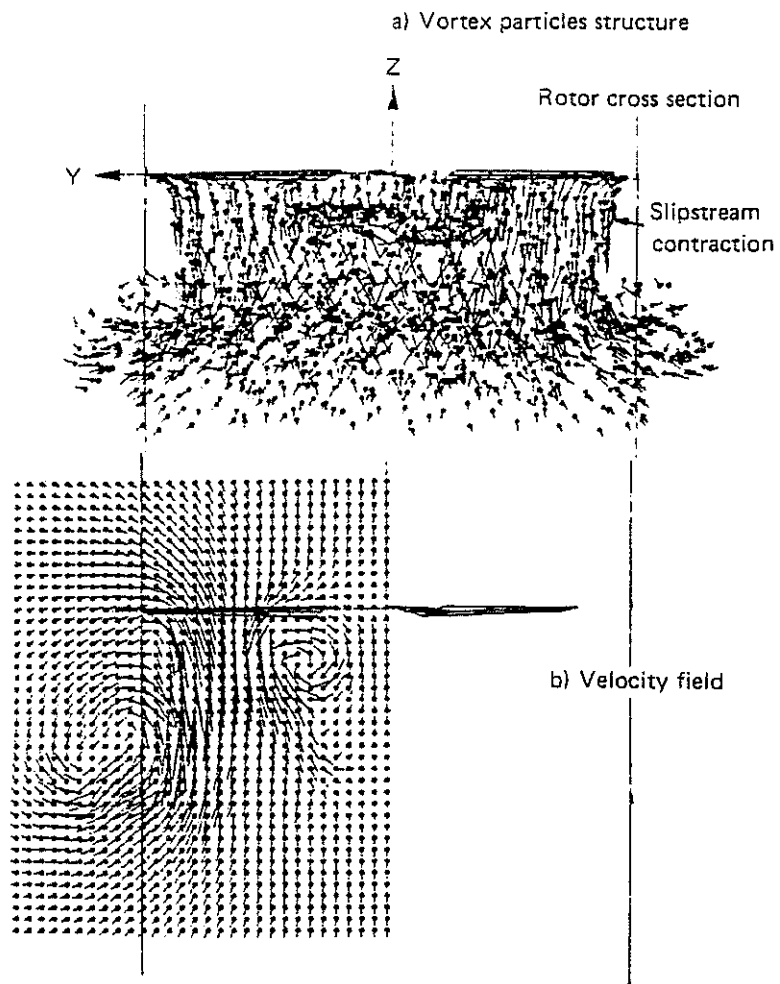

Fig. 9 — Thrust evolution in hovering flight.

a) Vortex particles structure

Z

Rotor cross section

Y

Slipstream
contraction

b) Velocity field

Fig. 10 — Initial axial starting wind technique.

Circulation

0.030

0.025

0.020

0.015

○ Pressure integration
◇ Potential jump at
   trailing edge
— Summa

Spanwise location r/R

0.3   0.5   0.7   0.9
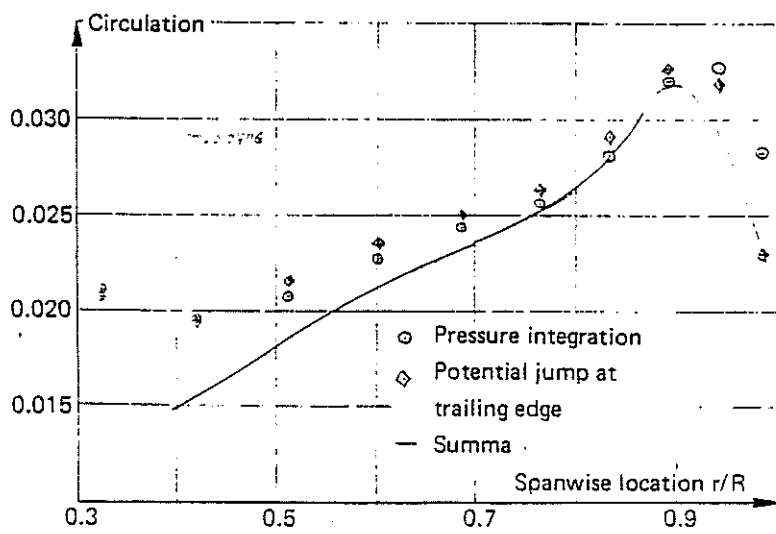
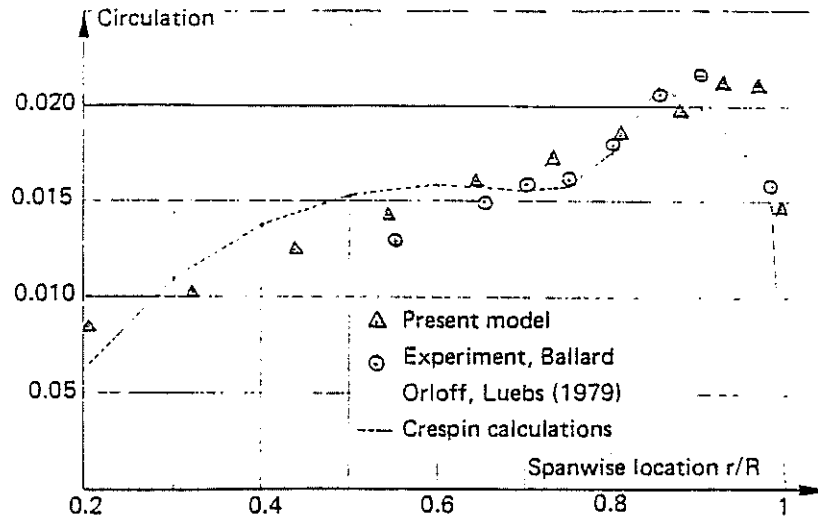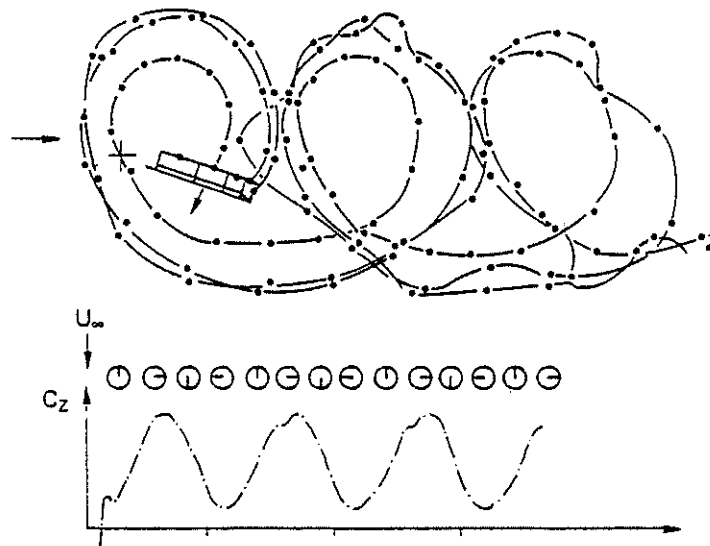*Fig. 11 — Sectional loading for a three-bladed rotor.*

Fig. 12 — Sectional loading for a two-bladed rotor.

Fig. 13 — One-bladed rotor in forward flight.